Nonoxidative Coupling of Ethane with Gold loaded Photocatalysts

AUTHOR(S):

Singh, Surya Pratap; Yamamoto, Akira; Yoshida, Hisao

ARTICLE

Nonoxidative Coupling of Ethane with Gold loaded Photocatalysts

Surya Pratap Singh,[a] Akira Yamamoto [ab] and Hisao Yoshida*[ab]

Received 00th January 20xx,
Accepted 00th January 20xx

DOI: 10.1039/x0xx00000x

Direct and continuous conversion of ethane to yield *n*-butane and hydrogen at near room temperature (*ca.* 320 K) was examined with gold loaded gallium oxide and titanium dioxide photocatalysts without the aid of any oxidant in a flow reactor. A Ga_2O_3 photocatalyst produced *n*-butane and ethene as well as hydrogen with almost stoichiometric ratio of products from ethane. Loading Au on the Ga_2O_3 sample gave 12 times higher production rate of *n*-butane such as 0.65 μmol h^{-1} with a high selectivity of 89 %. Although a bare TiO_2 sample showed very low yield due to poor reduction resistance, the addition of Au cocatalyst drastically improved the photocatalytic performance of the TiO_2 sample, i.e., an Au(0.2)/TiO_2 sample produced *n*-butane and ethene continuously at least for 5 h, where the production rate of *n*-butane, the *n*-butane selectivity, and the apparent quantum efficiency (AQE) for *n*-butane formation were 0.92 μmol h^{-1}, 92%, and 0.02%, respectively. The reaction mechanism of *n*-butane formation as a main reaction was proposed to be photocatalytic nonoxidative coupling of ethane (NOCE), which is similar to the photocatalytic nonoxidative coupling of methane (NOCM).

Introduction

Ethane is one of the main components of natural gas second only to methane.[1] Utilization of natural gas as a carbon source is of utmost importance and thus it is required to develop the conversion processes of not only methane but also ethane to the value-added chemicals. However, most of the processes to convert ethane are thermodynamically not feasible at room temperature due to the positive Gibbs energy change except for combustion or partial oxidation with oxygen.[2] Traditionally, ethane conversion has been studied in both the homogenous and the heterogeneous catalytic systems. Homogeneous conversion and functionalization of ethane involve harsh reaction conditions such as strong electrophiles, super acids, strong oxidants and require noble metals such as iridium, rhodium and ruthenium complexes.[3,4] On the other hand, heterogenous catalysis including oxidative coupling, aromatization, and CO_2 reforming of ethane requires high operating temperatures and thus suffers from high energy input and high cost.[5,6]

Alternatively, photocatalysis is a green technology to convert ethane via C–H bond activation to various chemicals under milder conditions.[2] A mercury-photosensitized decomposition of ethane at higher temperatures (673–773 K) to yield ethene and hydrogen as the major products can be considered the first report.[7] After that, various photocatalytic and photoinduced processes including homogeneous,[8] heterogeneous,[9–15] and supercritical ethane conversion[16] have been developed. Among them, the heterogenous photocatalytic pathway has been widely studied for ethane conversion with various oxidants such as O_2, CO_2, and NO to yield a variety of products ranging from CO,[9] CO_2,[10] C_2H_4,[11] formaldehyde,[12] acetaldehyde[12] to ethanol,[13] and so on.[14,15] However, much less effort has been devoted for the direct conversion of ethane into higher hydrocarbons like butane without aid of any oxidant.

In our studies of the photocatalytic nonoxidative coupling of methane (NOCM) for more than two decades,[17] ethane and hydrogen were obtained selectively as the main products with various photocatalysts such as the non-semiconductor photocatalysts[18] like Al_2O_3,[19,20] SiO_2-Al_2O_3,[19,20] SiO_2-Al_2O_3-TiO_2,[21,22] and Ce/SiO_2,[23] and also the semiconductor photocatalysts like Ga_2O_3,[24] Pd/Ga_2O_3,[25] and Pd-Bi/Ga_2O_3.[26] Particularly, the Pd-Bi/Ga_2O_3 photocatalyst showed the excellent stability with continuous production of ethane and hydrogen selectively for 100 h with high formation rates.[26] Recently, GaN and ZnO solid solution thin films showed good activity for the NOCM with high selectivity.[27] An Au/TiO_2 photocatalyst with light-diffuse-reflection-surfaces also promoted the NOCM selectively.[28] Thus, in the present study we tested whether or not the photocatalysts for the NOCM can efficiently convert ethane under nonoxidative conditions in a flow reactor. Among the examined several samples, the Au loaded Ga_2O_3 and TiO_2 photocatalysts showed the high activity to form *n*-butane in the nonoxidative direct ethane conversion under photoirradiation in the mild conditions, nearly room temperature and atmospheric pressure.

Experimental

[a] *Department of Interdisciplinary Environment, Graduate School of Human and Environmental Studies, Kyoto University, Yoshida Nihonmatsu-cho, Sakyo-ku, Kyoto 606-8501, Japan*
[b] *Elements Strategy Initiative for Catalysts and Batteries (ESICB), Kyoto University, Goryo-Ohara, Nishikyo-ku, Kyoto 615-8245, Japan*

† Footnotes relating to the title and/or authors should appear here.

Electronic Supplementary Information (ESI) available: [Experimental set-up, spectral output of Xe-lamp, calculations of yield, selectivity, $R_{CH/H2}$, and AQE, chromatograms, DR UV-vis spectrum of Al_2O_3, XRF analysis, additional XRD patterns, SEM images and EDX mappings, STEM images, and the DR UV-vis spectra of Au/TiO_2 samples, effect of thermal energy in the dark]. See DOI: 10.1039/x0xx00000x

Materials and Sample Preparation

The following chemicals employed in the present study were either obtained commercially or were donated by the Catalysis Society of Japan: Ga_2O_3 (99.90%, Kojundo Chemicals, the same reagent used in the previous work),[26] a mixture of rutile and anatase TiO_2 (P-25, 49 $m^2 g^{-1}$, Nippon Aerosil Co. Ltd.), and Al_2O_3 (JRC-ALO-7, γ-phase, 170 $m^2 g^{-1}$, the Catalysis Society of Japan). A Pd standard solution (5 mg mL^{-1} $Pd(NO_3)_2$ in 6.6 mol L^{-1} HNO_3(aq), Wako Chemicals) and a Bi standard solution (1 g L^{-1} $Bi(NO_3)_3$ in 0.5 mol L^{-1} HNO_3(aq), Wako Chemicals) were used as the precursors of Pd and Bi elements, respectively in the preparation of the Pd/Ga_2O_3 sample and the $Pd\text{-}Bi/Ga_2O_3$ sample by an impregnation and a co-impregnation method, respectively. The procedures of the preparation of Pd/Ga_2O_3 sample and the $Pd\text{-}Bi/Ga_2O_3$ sample were the same as described in our previous study.[26] The loading amount of Pd and Pd-Bi cocatalyst was 0.18 mol% for each element, which is also the typical value in the previous study.[26]

$HAuCl_4{\cdot}4H_2O$ was used as a precursor of the Au element. The Au loaded photocatalyst samples were prepared by the photodeposition method. A typical procedure for the preparation of an Au/TiO_2 sample is as follows. 1.2 g of TiO_2 (white powder) was dispersed in 48 mL of deionized water and this suspension was photoirradiated for 0.5 h. Then 12 mL of methanol and the required amount of the precursor of Au were added to this suspension and it was stirred for 1 h in dark. The suspension was then photoirradiated from a ceramic xenon lamp (PE300BUV, 300 W) for 0.5 h. The powder was then filtered, washed with water and ethanol, and dried in an electric oven at 373 K overnight. A purple-colored powder of Au/TiO_2 sample was obtained. A similar procedure was followed to prepare other Au loaded samples. The prepared samples were referred to as Au(*x*)/catalyst, where *x* in mol % gives the loading amount of Au.

Characterization

The obtained samples were characterized by several techniques. The crystal structure was determined by powder X-ray diffraction (XRD) with a Shimadzu LabX XRD-6000 X-ray diffractometer using Cu Kα radiation (40 kV, 30 mA). A Hitachi SU8220 model scanning electron microscope (SEM) in conjunction with a Horiba EX-370 energy dispersive X-ray (EDX) analyser was used to record the SEM images and EDX elemental mappings. Transmission electron microscope (TEM) and scanning transmission electron microscope (STEM) images were recorded in a high-angle annular dark field (HAADF) mode with a JEOL model JEM-2000FC field emission electron microscope. Diffuse reflectance UV-visible (DR UV-vis) spectra were recorded by a JASCO V-570 UV/VIS/NIR spectrophotometer equipped with an integrating sphere covered with a $BaSO_4$ reference. The loading amount of Au was determined by the X-ray fluorescence (XRF) analysis using a Shimadzu EDX-8000 energy dispersive X-ray fluorescence spectrometer. A calibration curve was made for XRF analysis with the Au/TiO_2 samples prepared by an impregnation method followed by calcination (673 K, 2 h) and it was used to determine the actual loading amount of Au in the Au/TiO_2 samples prepared by the photodeposition method in the present study. Au L_{III}-edge X-ray absorption fine structures (XAFS) of the Au/TiO_2 samples were measured in a fluorescence mode using a 19-element Ge solid state detector (SSD) at the BL12C beamline of synchrotron radiation facility Photon Factory, IMSS, KEK, Japan. The spectral output of the Xe-lamp (PE300BUV, 300W) was measured by a USB fiber optic spectrometer (USB2000 model, Ocean Optics).

Photocatalytic Reaction Test

The photocatalytic activity tests for the direct ethane conversion were carried out using a flow reactor similar to our previous works[25,26] as shown in Figure S1 in the supplementary information. The catalyst powder was pressed under 40 MPa pressure and ground into granules of 310–710 μm (25–50 mesh). The sample granules were filled into a quartz cell (2 × 2 × 0.1 cm^3, see the photograph in the inset of Figure S1). The weights of the granules used for filling the cell were 0.8, 0.6, and 0.4 g for the bare and cocatalysts loaded Ga_2O_3, TiO_2, and Al_2O_3 samples, respectively. The sample was pretreated with an argon flow for 30 min (flow rate 27 mL min^{-1}) to exclude the air from the quartz cell. A flow of mixture of 10% ethane in argon (total flow rate 30 mL min^{-1}) was introduced to the cell for 1 h in dark to achieve stable conditions, where the contact time was nearly 0.8 s and space velocity (SV) was 4500 h^{-1}. The sample was then photoirradiated from a ceramic xenon lamp (PE300BUV, 300 W, Figure S2) to start the reaction. The irradiation area was 4 cm^2 and the light intensity measured by a UV radiometer (Topcon, UD 250 detector) in the wavelength range of 220–300 nm with the highest sensitivity at 254 nm was *ca.* 20 mW cm^{-2}. During the photocatalytic reaction test, the temperature of the surface of the sample cell measured by an infrared thermometer (Testo, 835-T1) was increased to *ca.* 320 K by photoirradiation. The outlet gases were analyzed by two on-line gas chromatographs: one equipped with a TCD (Shimadzu, GC-8A, argon carrier, a Molecular Sieves 5A, column temperature 333 K) and another with an FID (Shimadzu, GC-8A, argon carrier, a Gaskuropack 54, column temperature 363 K). The detectable gases by the GC-TCD were hydrogen, oxygen, nitrogen, methane, ethene, ethane and carbon monoxide while the detectable gases by the GC-FID were methane, ethene, ethane, propene, propane, *i*-butane and *n*-butane in the detection range of retention times. The yield of the reaction is calculated as shown in eq. S1 in the supplementary information. The selectivity toward *n*-butane and ethene production was calculated based on ethane as shown in eq. S2 and S3, respectively in the supplementary information. The ratio of the produced hydrocarbons and hydrogen, $R_{HC/H2}$ is calculated as shown in eq. S4 in supplementary information. The apparent quantum efficiency (AQE) for *n*-butane and ethene production was calculated as shown in eq. S5[29] in the supplementary information.

Results and Discussion

Reaction Tests of Photocatalytic Direct Ethane Conversion

Table 1 Results of the reaction tests of photocatalytic direct ethane conversion[a]

Entry	Sample[b]	Production rates[c] / μmol h^{-1}				Yield[d]	S_{C4H10}[e]	S_{C2H4}[f]	$R_{HC/H2}$[g]
		C_4H_{10}	C_2H_4	CH_4	H_2	(%)	[NOCE]	[NODH]	
1	Ga_2O_3	0.054	0.057	trace[h]	0.097	0.002	65.5	34.5	1.1
2	Pd/Ga_2O_3	trace[h]	0.017	nd[i]	trace[h]	0.0003	–[j]	100	–[j]
3	Pd-Bi/Ga_2O_3	nd[i]	0.26	nd[i]	trace[h]	0.004	–[j]	100	–[j]
4[k]	Au(0.4)/Ga_2O_3	0.65	0.14	0.016	0.27	0.021	89.3	9.6	2.9
5	TiO_2	nd[i]	trace[h]	0.043	nd[i]	0.0006	–[j]	–[j]	–[j]
6[k]	Au(0.4)/TiO_2	0.77	0.33	0.031	0.69	0.028	81.0	17.4	1.5
7[l]	Al_2O_3	0.13	0.072	0.028	0.040	0.005	72.2	20.0	4.4
8	Au(0.4)/Al_2O_3	0.091	0.033	nd[i]	nd[i]	0.003	84.7	15.3	–[j]

[a]The reaction conditions were as follows, photocatalyst in a quartz cell = 0.8 g (Ga_2O_3, Pd/Ga_2O_3, Pd-Bi/Ga_2O_3, and Au/Ga_2O_3), 0.6 g (TiO_2 and Au/TiO_2), or 0.4 g (Al_2O_3 and Au/Al_2O_3); photoirradiation area = 4 cm^2; cell volume = 0.4 cm^3; feed gas = 10% of C_2H_6 in Ar (total flow rate 30 mL min^{-1}); contact time = 0.8 s; space velocity (SV) = 4500 h^{-1}; light intensity = *ca.* 20 mW cm^{-2}; reaction temperature = *ca.* 320 K. [b]The loading amount of Au was 0.4 mol% in entries 4, 6, and 8 while the loading amount of Pd and Bi each was 0.18 mol% in entries 2 and 3. [c]The production rates were measured 5.5 h later from the start of the photoirradiation. [d]Calculated hydrocarbon yield as shown in eq. S1. [e]Calculated as shown in eq. S2. [f]Calculated as shown in eq. S3. [g]Calculated as shown in eq. S4. [h]The amount of observed product was less than 0.01 μmol h^{-1}. [i]nd = not detected. [j]Could not be calculated. [k]The reaction tests were done three times and the average values are given here. [l]Very small amounts of many other products like CO, C_3H_6, and C_3H_8 were also detected.

Several samples were examined for the reaction tests of photocatalytic direct ethane conversion in a flow reactor and the results are given in Table 1. The main products observed were *n*-butane, ethene, and methane as well as hydrogen, while very small amounts of other hydrocarbon products such as propene and propane were also found in some cases. No *i*-butane was detected. The representative chromatograms of the GC-TCD and GC-FID after the reaction tests of the photocatalytic direct ethane conversion showing the peaks of various products and the reactant in the reaction are shown in Figure S3 and Figure S4, respectively.

n-Butane would be formed via photocatalytic nonoxidative coupling of ethane with hydrogen formation (NOCE, eq. 1) in the same way as nonoxidative coupling of methane (NOCM) in the present conditions. This is a thermodynamically unfavourable reaction with the positive Gibbs energy change.

$$2\ C_2H_6 \rightarrow C_4H_{10} + H_2 \qquad \Delta_rG_{298K} = 48.6\ kJ\ mol^{-1} \qquad (1)$$

Ethene should be formed via photocatalytic dehydrogenation of ethane (DH), where nonoxidative (eq. 2) or oxidative (eq. 3) pathways are possible. In the former case of nonoxidative dehydrogenation (NODH), ethene and hydrogen are produced, which is also a thermodynamically unfavourable reaction with a much larger value of the positive Gibbs energy change than the NOCE. In the latter case of oxidative dehydrogenation (ODH), the lattice oxygen (O_L) of the photocatalyst surface is tentatively assumed as the oxidant and ethene and water would be formed.

$$C_2H_6 \rightarrow C_2H_4 + H_2 \qquad \Delta_rG_{298K} = 101\ kJ\ mol^{-1} \qquad (2)$$

$$C_2H_6 + O_L \rightarrow C_2H_4 + H_2O \qquad (3)$$

Methane as a very minor product would be formed via hydrocracking (HDC) of ethane with hydrogen (eq. 4) as the reverse reaction of NOCM, where hydrogen should be supplied via the NOCE and the NODH (eqs. 1 and 2). Another possible reaction would be oxidative route with the reduction of photocatalyst surface via partial oxidation of ethane to acetic acid and its decomposition[30] (eq. 5) although CO_2 was not detected due to very low sensitivity in the present conditions.

$$C_2H_6 + H_2 \rightarrow 2\ CH_4 \qquad \Delta_rG_{298K} = -68.6\ kJ\ mol^{-1} \qquad (4)$$

$$C_2H_6 + 3O_L \rightarrow CH_3COOH + H_2O \rightarrow CH_4 + CO_2 + H_2O \qquad (5)$$

In the present reaction system, no products were observed in the dark, without the photocatalyst, and without ethane in the feed gas, meaning that these reactions would be photocatalytic or photo-induced reactions and the products would be derived from ethane.

Gallium oxide (Ga_2O_3) is a well-studied material as both catalyst[31–33] and photocatalyst[34–37] for hydrocarbon conversions, which was stable even in the present reductive reaction conditions in contrast to the TiO_2 sample as mentioned later.[25,26] The Ga_2O_3 sample produced *n*-butane, ethene, and hydrogen with the production rates of 0.054, 0.057, and 0.097 μmol h^{-1}, respectively (Table 1, entry 1). The observed hydrogen production rate was comparable to the sum of the production rates of *n*-butane and ethene since both the NOCE and the NODH reactions provide hydrogen as a product and the ratio of hydrocarbons and hydrogen was close to unity, $R_{HC/H2}$=1.1, meaning that these NOCE and NODH reactions proceeded with the stoichiometric ratio of the products without by-products. The production rates of *n*-butane and ethene are almost the same. These facts suggest that both the NOCE and the NODH reactions selectively and competitively occurred (eq. 1 and 2) over the Ga_2O_3 sample. The selectivity based on ethane to form *n*-butane was high such as 65.5%.

Since in our previous studies, Pd/Ga_2O_3 and Pd-Bi/Ga_2O_3 photocatalysts showed high activity with high selectivity for the NOCM,[25,26] these samples were prepared following the same procedures with the same loading amount described in our last study[26] and examined for the photocatalytic direct ethane conversion. Contrary to expectations, only a small amount of ethene was observed over these samples with trace amount of hydrogen (Table 1, entries 2–3), indicating that these samples are not efficient for the photocatalytic direct ethane conversion to butane. Although the DH reaction proceeded, the NOCE did not take place on the Pd-Bi/Ga_2O_3 sample at all. This result suggests that the required property for the NOCE is not the same as that for the NOCM and the same photocatalyst could not be always efficient for further conversion of the product in the NOCM. In addition, it is expected that these photocatalysts can promote the NOCM selectively without successive coupling of the product.

Gold (Au) is used as a cocatalyst for the photocatalysts in the methane conversion reactions such as the NOCM,[28,38] and the oxidative methane conversion,[39,40] and also in other reactions like organic chemical conversions.[41] It was found that loading of Au cocatalyst on the Ga_2O_3 sample resulted in an increase of the yield, over which *n*-butane, ethene, methane and hydrogen were produced (Table 1, entry 4). *n*-Butane was obtained as the major hydrocarbon product in photocatalytic direct ethane conversion over the Au(0.4)/Ga_2O_3 sample with its production rate and selectivity being 0.65 μmol h^{-1} and 89.3%, respectively, and the production rate of *n*-butane was 12 times higher than that over the bare Ga_2O_3 sample, meaning that the Au(0.4)/Ga_2O_3 sample efficiently and selectively promotes the NOCE.

Titanium dioxide (TiO_2) is a representative photocatalyst.[28,42] The bare TiO_2 sample mainly yielded methane with a trace amount of ethene without formation of hydrogen and butane (Table 1, entry 5). The color of the bare TiO_2 sample varied from white (Figure 1a) to blue (Figure 1b) during the reaction, especially at the downstream part.

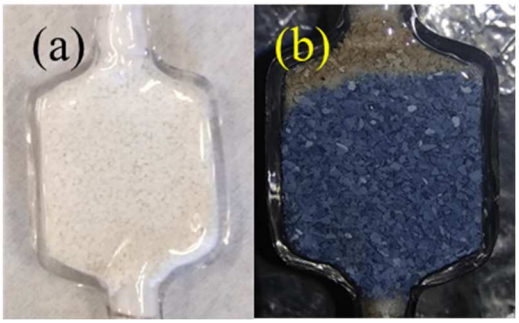

Figure 1 Photographs of the sample cell (a) before and (b) after the reaction test of photocatalytic ethane conversion with bare TiO_2 sample. The photograph in b was taken before removing the reactor from the set-up.

The lack of hydrogen formation and the color change suggest that TiO_2 is reduced by ethane and the produced hydrogen, i.e., TiO_2 is unstable in the reductive reaction conditions under photoirradiation. Thus, the most plausible reaction would be a combination of partial oxidation of ethane with the surface oxygen and decomposition of acetic acid (eq. 5) as well as reduction of the TiO_2 surface by ethane. Loading of Au cocatalyst drastically increased the activity of the TiO_2 sample also. The Au(0.4)/TiO_2 sample exhibited the high production rate of *n*-butane and ethene, 0.77 and 0.33 μmol h^{-1}, respectively (Table 1, entry 6), which were higher than those over the Au(0.4)/Ga_2O_3 sample. The Au(0.4)/TiO_2 sample showed the highest products yield among all the samples given in Table 1. Over the Au(0.4)/TiO_2 sample also, *n*-butane was the major hydrocarbon product and its selectivity was 81.0%, meaning that the NOCE was also the major pathway of product formation in the photocatalytic direct ethane conversion over the Au(0.4)/TiO_2 sample. This high performance for the NOCE is consistent with the report of Au loaded TiO_2 photocatalyst as a good photocatalyst for the NOCM.[28] Here, it is to be noted that the Au loaded TiO_2 as an efficient photocatalyst for the NOCM also showed good performance for the NOCE while the Pd-Bi loaded Ga_2O_3 photocatalyst did not. Thus, a photocatalyst active for the NOCM is not always active for the NOCE and it would depend on the intrinsic properties of the photocatalyst material itself. The Pd/Ga_2O_3 and Pd-Bi/Ga_2O_3 photocatalysts tended to yield not butane but ethene, suggesting these samples enhanced ethane conversion according to a different mechanism. This might be related to the catalytic properties of Ga_2O_3 in hydrocarbon conversion.[43]

Aluminium oxide (Al_2O_3) is usually used as an insulator support and acid-base catalyst,[44] while it has also photocatalytic property for the NOCM as mentioned above.[19,20] In the present reaction, it produced *n*-butane, ethene, methane and hydrogen with a selectivity of *n*-butane and ethene of 72.2% and 20.0%, respectively (Table 1, entry 7). Other products such as carbon monoxide, propene and propane were also observed with Al_2O_3 meaning that the mechanism of photocatalytic ethane conversion on the insulator support such as Al_2O_3 is different from that on the semiconductor photocatalyst such as Ga_2O_3 and TiO_2. A small absorption was shown by the bare Al_2O_3 in the DR UV-vis spectrum (Figure S5). A similar absorption is reported in the literature.[45] Besides, Al_2O_3 has many acid and base sites[44] and the hydroxyl groups on the surface of Al_2O_3 are sometimes considered responsible for its photoactivity.[46] The light can be absorbed by these surface species and then this photoenergy can be transferred to the adsorbed ethane molecules resulting in the formation of products by photocatalytic reactions. In contrast to the above cases, loading of the Au cocatalyst decreased the photocatalytic performance of the bare alumina (Table 1, entry 8). The photocatalytic active sites and the reaction mechanism on the alumina surface would be definitely different from those on the semiconductor photocatalyst, i.e., the surface sites are excited by photon to promote the reactions and the Au particles would disturb the surface activity.

Among several samples, the Au(0.4)/TiO_2 sample exhibited the highest photocatalytic performance. Thus, further investigation was carried out on the Au/TiO_2 photocatalysts.

Table 2 Optimization of the loading amount of Au in the Au(x)/TiO_2 samples[a]

Entry	Loading amount (mol%)	Production rates[b] / μmol h^{-1}				Yield[c] (%)	S_{C4H10}[d] [NOCE]	S_{C2H4}[e] [NODH]	$R_{HC/H2}$[f]
		C_4H_{10}	C_2H_4	CH_4	H_2				
1[g]	0	nd[h]	trace[i]	0.043	nd[h]	0.0006	–[j]	–[j]	–[j]
2	0.10	2.05	0.090	0.083	0.47	0.062	95.9	2.1	4.4
3	0.20	0.92	0.11	0.055	0.63	0.029	91.8	5.5	1.5
4	0.40	0.77	0.33	0.031	0.69	0.028	81.0	17.4	1.5
5	1.0	0.64	0.28	0.030	0.60	0.023	80.5	17.6	1.5

[a]The reaction conditions were same as those described in the footnote *a* of Table 1. [b]Production rates were measured after 5.5 h. [c]Calculated as shown in eq. S1. [d]Calculated as shown in eq. S2. [e]Calculated as shown in eq. S3. [f]Calculated as shown in eq. S4. [g]Bare TiO_2 sample (P-25) was used in the reaction test and this is the same result listed in Table 1, entry 5. [h]nd = not detected. [i]The amount of observed product was less than 0.01 μmol h^{-1}. [j]Could not be calculated.

Optimization of Loading Amount of Au

The loading amount of Au cocatalyst is varied in the Au(x)/TiO_2 samples, where the loading amount was confirmed to be correct by XRF as shown in Table S1. The results of the photocatalytic activity tests are shown in Table 2. As opposed to a very small activity with the bare TiO_2 sample (Table 2, entry 1 and also Table 1, entry 5), the activity increased after depositing Au cocatalyst on the TiO_2 sample (Table 2, entries 2–5).

A very small amount of Au deposition of 0.1 mol% much increased the yield of the reaction and the *n*-butane formation rate of 2.05 μmol h^{-1} with the selectivity of 95.9% were observed although the value of *R* was high (Table 2, entry 2).

On increasing the loading amount to 0.20–1.0 mol%, the yield of the reaction decreased but the value of *R* was improved (Table 2, entries 3–5). Among them, the Au(0.2)/TiO_2 sample showed the best performance with the higher production rates and selectivity of *n*-butane of 0.92 μmol h^{-1} and 91.8 %, respectively with a moderate value of *R* of 1.5 (Table 2, entry 3). The apparent quantum efficiency (AQE) for *n*-butane formation via the NOCE was calculated to be 0.02 % over the Au(0.2)/TiO_2 photocatalyst assuming that two photons were used to form one butane molecule as discussed later. The yield of the reaction was calculated to be 0.029 % with the Au(0.2)/TiO_2 sample.

Although the bare TiO_2 sample was not stable under the reductive reaction conditions and showed no production of hydrogen as mentioned above, after loading the Au cocatalyst we could observe hydrogen with the Au/TiO_2 samples and the value of $R_{HC/H2}$ was improved to be 1.5 when the loading amount was equal to or higher than 0.2 mol%. This suggests that the loaded Au species on the surface reacts with the unstable sites of the TiO_2 surface to stabilize it as a result, i.e., the stabilized moieties are scarcely reduced under the reaction conditions or does not take part in the oxidative reactions such as eq. 3 and 5. The number of such stabilized moieties would depend on the loading amount of the Au cocatalyst, i.e., 0.2 mol% of Au loading would be enough to diminish the unstable surface sites and thus the value of $R_{HC/H2}$=1.5, close to an ideal value, was obtained (Table 2, entries 3–5), while a small amount of Au such as 0.1 mol% would not be enough and thus a high value of $R_{HC/H2}$ was obtained (Table 2, entry 2). Such kind of interfacial structure of Au/TiO_2 sample is previously also suggested based on both experimental results[47] and the theoretical calculations.[48,49] It is also reported that a low Au content will enable the small Au species to be imbedded in the surface structure while a high Au content will increase the particle size and give the nanoparticles on the surface.[47] Over all the Au/TiO_2 samples, the NOCE to form *n*-butane was the major reaction pathway with the high selectivity being in the range of 96–80 %.

However, the reaction selectivity to *n*-butane formation varied with the Au loading amount. With the increase of the Au loading from 0.1 to 0.4 mol%, the yield and selectivity for the NOCE decreased while those for the NODH to form ethene increased. The ethene production rate was the highest on the Au(0.4)/TiO_2 photocatalyst, 0.33 μmol h^{-1}. The AQE for ethene formation on the Au(0.4)/TiO_2 was 0.008 %, where tentatively a two photon process was assumed for the calculation.

We studied the variation of the products formation with time in the photocatalytic direct ethane conversion reaction and Figure 2A shows the time course of the production rates with the Au(0.4)/TiO_2 sample as a typical example. The production rates decreased in the beginning and then tended to become stable after 5.5 h of the photoirradiation so that the values at 5.5 h later were listed in Table 1 and Table 2, i.e., the production rates of *n*-butane, ethene, methane and hydrogen were 0.77, 0.33, 0.031, and 0.69 μmol h^{-1}, respectively after 5.5 h with the yield of the reaction being 0.028%. The trend of the reaction selectivity to *n*-butane and ethene as well as the *R* value did not change much with time (Figure 2B). However, the activity of the sample decreased in the beginning as shown in Figure 2A. This decrease might be due to the increase in the particle size of Au

nanoparticles from its aggregation in the Au(0.4)/TiO_2 sample during the reaction as discussed later.

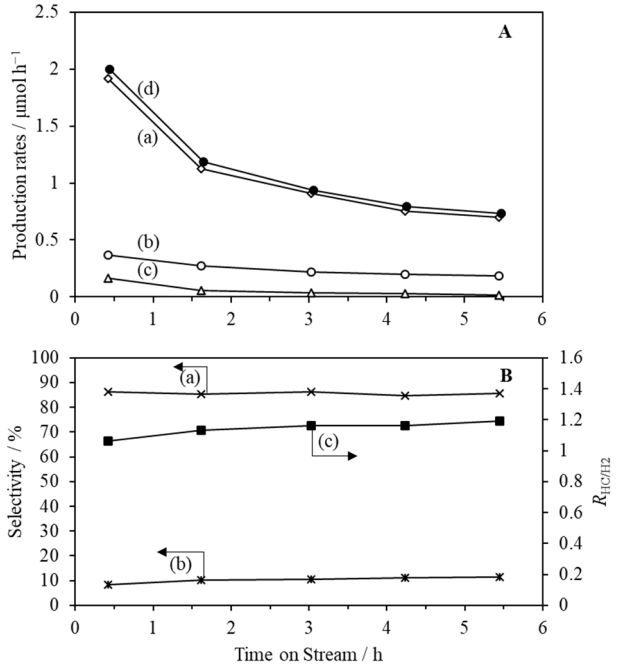

Figure 2 (A) Time course of production rates of (a) *n*-butane, (b) ethene, (c) methane, and (d) hydrogen, and (B) time course of selectivity toward (a) *n*-butane, (b) ethene, and (c) the $R_{CH/H2}$ value, in the reaction test of photocatalytic direct ethane conversion with the Au(0.4)/TiO_2 photocatalyst. Reaction conditions were same as those described in the footnote *a* of Table 1.

Characterization

We characterized the Au/TiO_2 samples by some techniques.

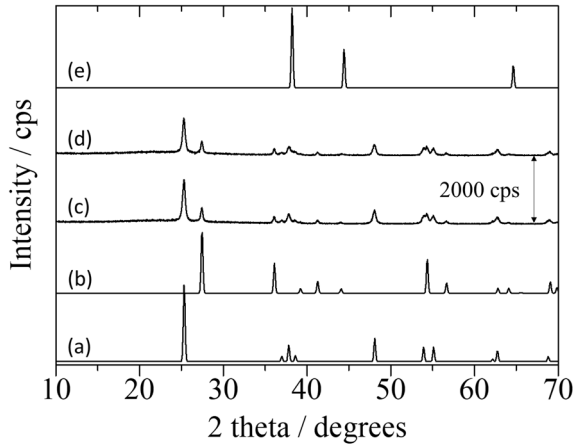

Figure 3 XRD patterns of (a) anatase TiO_2 from a database (ICSD #9852), (b) rutile TiO_2 from the database (ICSD #9161), (c) the TiO_2 sample, (d) the Au(0.4)/TiO_2 sample, and (e) Au from the database (ICSD #52249).

The XRD patterns of various samples are shown in Figure 3. The employed TiO_2 sample (P-25) was a mixed crystal of anatase and rutile phases and it was evident in its XRD pattern (Figure 3c) which consisted of the lines of both the anatase phase (Figure 3a, ICSD #9852)[50] and the rutile phase (Figure 3b, ICSD #9161)[51] with no additional lines. After loading of the Au cocatalyst in Au(0.4)/TiO_2 sample, a very broad and ambiguous diffraction line at 38.2° overlapping with those of anatase TiO_2 was observed (Figure 3d), which is assignable to the main diffraction of metallic Au (Figure 3e, ICSD #52249).[52] This observation suggests that the Au cocatalyst loaded by the photodeposition method was in metallic state in the Au(0.4)/TiO_2 sample. The XRD patterns of other Au/TiO_2 samples are given in Figure S6. The diffraction lines derived from the Au nanoparticles further became evident in the XRD patterns of the Au(1.0)/TiO_2 sample (Figure S6 e). The SEM image of the TiO_2 sample and the SEM image and EDX elemental mappings of the Au(0.4)/TiO_2 samples are shown in Figure S7. The agglomerated nanoparticles of TiO_2 were observed with no regular shape (Figure S7 a). The morphology did not change much after depositing Au species in the Au(0.4)/TiO_2 sample (Figure S7 b). The elemental mappings of the Au(0.4)/TiO_2 sample showed that Au nanoparticles were dispersed on TiO_2 surface (Figure S7 c-e).

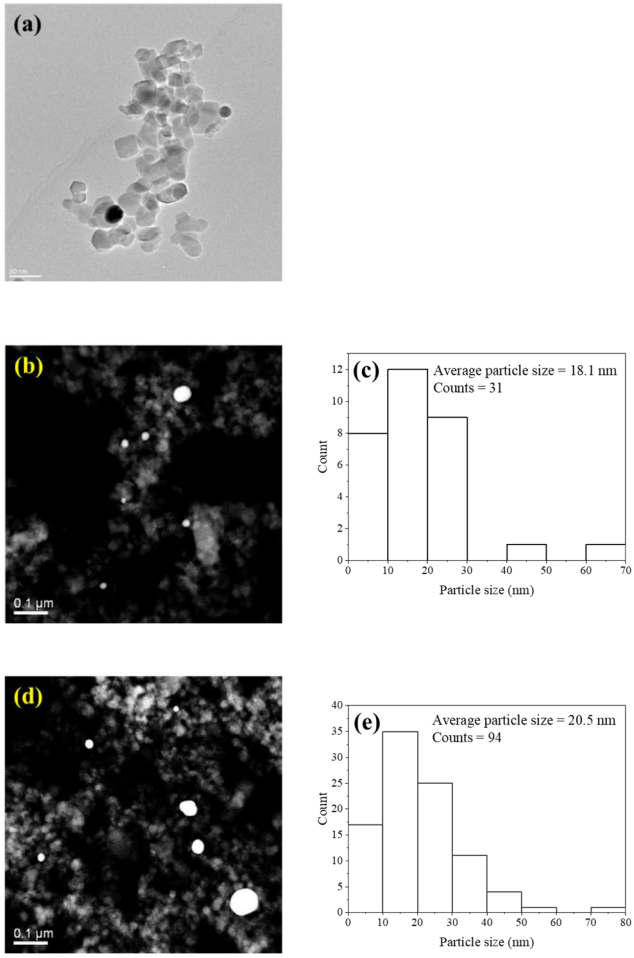

Figure 4 (a) TEM image, (b) STEM image and (c) particle size distribution in the Au(0.4)/TiO_2 sample before the use for the reaction test; and (d) STEM image and (e) particle size distribution of the Au(0.4)/TiO_2 sample after the use for the reaction test.

We further recorded the TEM and STEM images of various Au/TiO_2 samples in order to know the particle size of Au nanoparticles. Spherical Au nanoparticles can be seen in the

TEM image of the Au(0.4)/TiO_2 sample (Figure 4a). In the STEM image, Au nanoparticles can be distinguished very easily due to its high contrast to the TiO_2 nanoparticles (Figure 4b). The particle size distribution of Au nanoparticles clarified the average particle size to be 18.1 nm in Au(0.4)/TiO_2 sample (Figure 4c). The average particle size of Au nanoparticles increased to be 20.5 nm after the reaction (Figure 4d, e). The STEM images and the particle size distribution of other Au/TiO_2 samples are given in Figure S8. The average particle size of the Au nanoparticles increased with an increase in the loading amount of Au in the Au/TiO_2 samples.

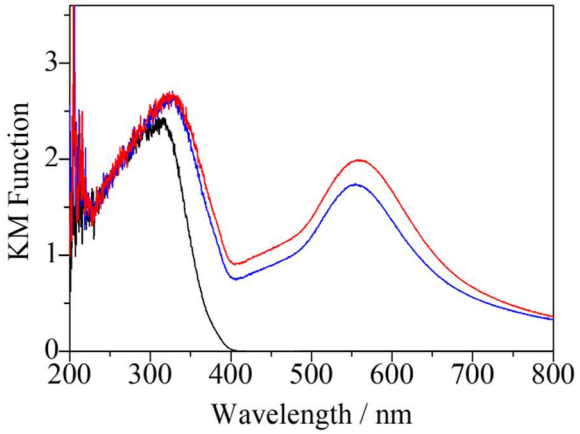

Figure 5 DR UV-vis spectra of the TiO_2 sample (black line) and the Au(0.4)/TiO_2 sample before (blue line) and after (red line) the use for the reaction test of photocatalytic direct ethane conversion.

The photoabsorption properties of the samples were investigated by the DR UV-vis spectroscopy. The bare TiO_2 sample showed a large absorption band below 400 nm in the wavelengths (Figure 5, black line) from which its band gap was calculated to be around 3.6 eV, which is in agreement with the literature.[28] The Au(0.4)/TiO_2 sample exhibited an additional intense and broad band centred at nearly 550 nm (Figure 5, blue line), which is assignable to the localized surface plasmon resonance (LSPR) band of metallic Au nanoparticles.[28] The tailing part of this LSPR band at shorter wavelength overlapped with the large band of TiO_2, which made the position of the absorption edge to be slightly shifted to longer wavelength. This means that the Au cocatalyst existed as metallic nanoparticles on the TiO_2 surface in Au(0.4)/TiO_2 sample, in agreement with its XRD profile (Figure 3d). We also recorded the DR UV-vis spectra of the Au(0.4)/TiO_2 sample after using for the photocatalytic reaction test. The intensity of the characteristic Au LSPR peak is increased and its position is slightly red-shifted (Figure 5, red line), which indicates the increase in the particle size of Au nanoparticles during the photocatalytic reaction test.[53] Thus, the results in the DR UV-vis spectra were in agreement with the STEM results for the increase in the particle size after the reaction test. The DR UV-vis spectra of other Au/TiO_2 samples are shown in Figure S9. All the Au/TiO_2 samples showed the absorption band due to the LSPR of the Au nanoparticles and the intensity of this band increased with an increase in the loading amount of Au cocatalyst. This is an expected trend since the number of the Au nanoparticles should be increased with an increase of loading amount of Au cocatalyst from an increase in the number and sizes of the Au nanoparticles.

The Au L_{III}-edge XAFS spectra of the Au foil and the Au(0.4)/TiO_2 samples is shown in Figure 6A. The shape of the XAFS spectra of the Au(0.4)/TiO_2 sample (Figure 6A, green line) was similar to that of the Au foil (Figure 6A, black line), suggesting that the state of the Au cocatalyst in the Au(0.4)/TiO_2 sample was metallic. The used sample for the photocatalytic reaction test exhibited almost the same XAFS spectra (Figure 6A, red line), indicating that the chemical state of the gold didn't change during the reaction in the Au(0.4)/TiO_2 sample. The Au L_{III}-edge k^3-weighted Fourier Transform (FT) EXAFS of the Au(0.4)/TiO_2 sample before and after the reaction is shown in Figure 6B. The peak in the range of 2.0–3.0 Å corresponds to the Au–Au bond[54] and the intensity of this peak is slightly increased after the reaction (Figure 6B, red line). This increase in the intensity is due to the increase of the particle size of Au nanoparticles.[54] Thus, the EXAFS results further support the DR UV-vis results.

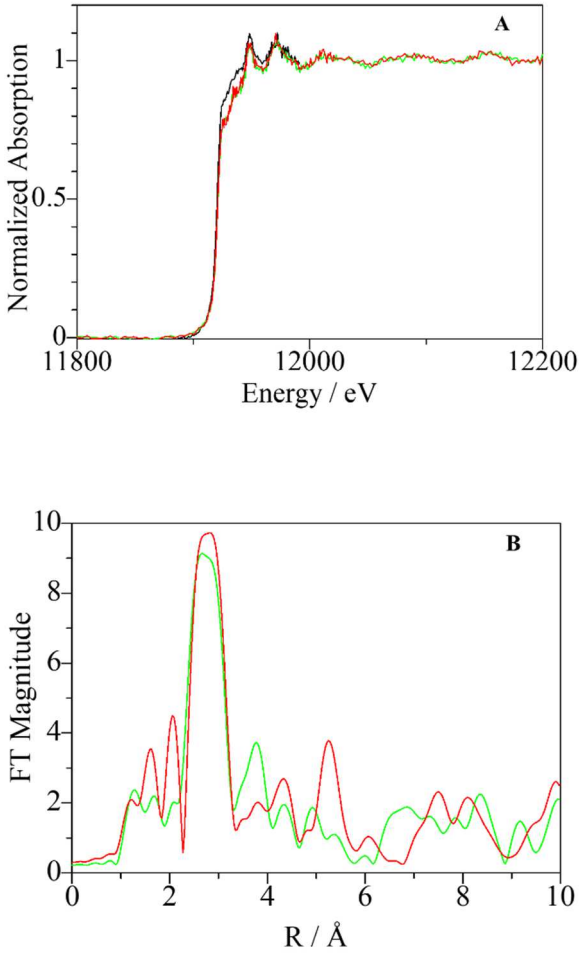

Figure 6 (A) Au L_{III}-edge XANES spectra of the Au foil (black line), Au(0.4)/TiO_2 sample before (green line) and after (red line) the use for the reaction test, and (B) Fourier Transform of EXAFS of Au(0.4)/TiO_2 sample before (green line) and after (red line) the use for the reaction test of photocatalytic direct ethane conversion.

Reaction Test with Optical Filter

As mentioned above, the Au cocatalyst was present as metallic Au nanoparticles on the Au(0.4)/TiO_2 photocatalyst and showed the intense LSPR band centred at nearly 550 nm in its DR UV-vis spectrum (Figure 5, blue line). It is well known that the LSPR can contribute to the photocatalytic activity.[38,55–57] In order to know whether or not this absorption contributed to the reaction, an additional reaction test was carried out with an optical filter passing light of wavelengths larger than 440 nm and the results are given in Table 3. As opposed to the high activity with no optical filter (Table 3, entry 1), a trace amount of ethene and no other products were observed when the optical filter ($\lambda_{transmission} \geq 440$ nm) was used (Table 3, entry 2). This result indicates that the LSPR of the Au nanoparticles did not contribute to the reaction without photoexcitation of the TiO_2 photocatalyst and the photoexcitation of TiO_2 was required for the photocatalytic reactions over the Au(0.4)/TiO_2 sample. This result is in agreement with the Au/TiO_2 photocatalyst for NOCM.[28]

Table 3 Result of the reaction tests of photocatalytic direct ethane conversion with an optical filter over the Au(0.4)/TiO_2 sample [a]

Entry	Conditions	Production rates[b] / μmol h^{-1}			
		C_4H_{10}	C_2H_4	CH_4	H_2
1	without filter	0.77	0.33	0.031	0.69
2	with filter	nd[c]	trace[d]	nd[c]	nd[c]

[a]The reaction conditions were same as those described in the footnote *a* of Table 1, except for the use of the optical filter ($\lambda_{transmission} \geq 440$ nm) in entry 2. [b]Production rates were measured after 5.5 h of the photoirradiation. [c]nd = not detected. [d]The amount of the product was less than 0.01 μmol h^{-1}.

Effect of Thermal Energy

Recently, photothermal catalytic reactions on supported metal catalysts have been reported,[58–60] where the light energy absorbed by the metal nanoparticles is converted to thermal energy to promote the catalysis on the metal catalyst. Thus, the reaction tests in the dark were carried out with the Au(0.4)/TiO_2 sample at various temperatures in the flow of ethane with Ar carrier gas to study the effect of thermal energy on the reaction. The results are given in Table S2 in the supplementary information. No products were observed at 323, 373, 423, and 473 K (Table S2, entries 1–4), meaning that ethane could not be activated by the thermal energy provided at these temperatures in the dark over the Au(0.4)/TiO_2 sample under the present reaction conditions. When we increased the temperature further, ethene, methane and hydrogen were produced on the Au(0.4)/TiO_2 sample and their production rates increased with increasing the temperature in the range of 523–723 K (Table S2, entry 5–9), which is consistent with literatures,[43] while no *n*-butane was formed in dark even at these temperatures. It was clear that the product distribution in the thermal reaction was not the same as under photoirradiation. Further, this result confirmed that the formation of *n*-butane via the NOCE proceeded photocatalytically under photoirradiation while the dehydrogenation of ethane to ethene can be promoted by thermal energy on the Au catalyst in dark. Thus, it is suggested that at least the NOCE was not photothermal reaction but photocatalytic reaction.

The similar product distribution and the variation with increasing temperature were also observed on the Au(0.4)/Ga_2O_3 sample (Table S3), where the production rate of ethene was almost equal to that of hydrogen, confirming that ethane dehydrogenation was selectively promoted over the Au catalyst supported on the Ga_2O_3 surface. Under photoirradiation, the production rates of ethene were 0.14 and 0.33 μmol h^{-1} over the Au(0.4)/Ga_2O_3 and Au(0.4)/TiO_2 samples, respectively as mentioned above (Table 1). These production rates of ethene correspond to those obtained in dark at 560 and 624 K with the Au(0.4)/Ga_2O_3 sample and the Au(0.4)/TiO_2 sample, respectively; where these temperatures were estimated according to Arrhenius equation based on the results in Table S2 and Table S3. The Xe lamp emits the continuous light in the wavelength range of UV and visible light (Figure S2) and there is a possibility of conversion of visible light to heat. Thus, if the local temperature of the Au nanoparticles were 560 and 624 K under photoirradiation, it is possible to explain that under photoirradiation ethene might be produced through ethane dehydrogenation catalysed by the Au nanoparticles[61] on these supports with thermal energy converted from photoenergy.

Reaction Pathways

At least, in the present study, it is clarified that the nonoxidative coupling of ethane (NOCE) was promoted photocatalytically. The reaction scheme of the NOCE would be proposed as follows: TiO_2 and Ga_2O_3 acting as the semiconductor photocatalysts can absorb the photons upon irradiation and electrons and holes are generated at their conduction band (CB) and valence band (VB), respectively. Ethyl radicals and protons are oxidatively produced by the photogenerated holes (eq. 6), and *n*-butane is formed by the coupling of two ethyl radicals (eq. 7), while hydrogen is reductively formed by the photogenerated electrons (eq. 8).

$$2C_2H_6 + 2h^+ \rightarrow 2\ {}^\bullet C_2H_5 + 2H^+ \quad (6)$$

$$2\ {}^\bullet C_2H_5 \rightarrow C_4H_{10} \quad (7)$$

$$2H^+ + 2e^- \rightarrow H_2 \quad (8)$$

As for the formation of ethene as a by-product, it is proposed that Au metal nanoparticles may promote dehydrogenation of ethane to ethene (eq. 2) as a catalyst[61] by the thermal energy that was converted from the photoenergy, while the possibility of photocatalytic dehydrogenation also could not be ruled out, for examples by using one photon (eq. 9–12) or by using two photons (eq. 9, 10, 12–13) including a disproportionation of ethyl radical (eq. 13).[62] Further careful investigation is required to clarify how the side reaction to form ethene took place under photoirradiation.

One photon process

$$C_2H_6 + h^+ \rightarrow {}^\bullet C_2H_5 + H^+ \quad (9)$$

$$H^+ + e^- \rightarrow H^\bullet \quad (10)$$

$${}^\bullet C_2H_5 \rightarrow C_2H_4 + H^\bullet \quad (11)$$

$$H^\bullet + H^\bullet \rightarrow H_2 \quad (12)$$

Two photon process

$${}^\bullet C_2H_5 + {}^\bullet C_2H_5 \rightarrow C_2H_4 + C_2H_6 \quad (13)$$

Conclusions

Photocatalytic direct conversion of ethane under nonoxidative conditions was studied in a flow reactor, and it was found that *n*-butane and hydrogen can be produced as the major products with the bare Ga_2O_3 photocatalyst, the Au-loaded Ga_2O_3 photocatalyst, and the Au-loaded TiO_2 photocatalysts, which is photocatalytic nonoxidative coupling of ethane (NOCE). Ethene and methane were also observed as additional hydrocarbon products.

The stability of the photocatalyst under the reductive reaction conditions is an important parameter in conjunction with the NOCM and so the Ga_2O_3 photocatalyst showed production of *n*-butane, ethene and hydrogen in nearly stoichiometric ratio. The Au(0.4)/Ga_2O_3 photocatalyst exhibited 12 times higher production of *n*-butane than the bare Ga_2O_3 photocatalyst along with hydrogen from ethane with the NOCE being the major reaction pathway and the selectivity to *n*-butane was as high as 89%.

Although the TiO_2 photocatalyst was not useful for the NOCE in the present conditions, the Au(0.2)/TiO_2 photocatalyst exhibited a higher photocatalytic activity for the NOCE, giving a high apparent quantum efficiency for *n*-butane formation such as AQE=0.02%, a high NOCE selectivity of 92%, and a moderate $R_{HC/H2}$ value of 1.5 and the yield of the reaction was 0.029 %.

The reaction mechanism of the photocatalytic NOCE to produce *n*-butane from ethane via radical-radical coupling would be similar to that of the NOCM to form ethane from methane while other reactions than the NOCE can take place in the photocatalytic direct conversion of ethane under nonoxidative conditions. Although the yield of ethene from ethane as one of the side reactions was also valuable, the mechanism of the ethene formation was unclarified, i.e., it remains possible that a photothermal dehydrogenation might take place under photoirradiation in the present conditions over supported Au catalysts.

Efforts to increase the production rate and the selectivity are needed for the further development of the photocatalytic direct conversion of ethane, and further detailed and careful investigations are required to clarify the reaction mechanisms.

Author Contributions

Surya Pratap Singh: Conceptualization, Investigation, Writing – original draft; Akira Yamamoto: Funding acquisition, Methodology; Hisao Yoshida: Conceptualization, Funding acquisition, Project Administration, Supervision, Writing – review and editing.

Conflicts of interest

There are no conflicts to declare.

Acknowledgements

The authors thank Mr. Tsutomu Kiyomura (Institute for Chemical Research, Kyoto University) for the measurements of the TEM and STEM images. A part of this work was supported by “Nanotechnology Platform” project of the MEXT, Japan, Grant Number JPMXP09A21KT0030. The XAFS spectra of the samples were measured at the BL12C of the Photon Factory (PF) with the approval of the Photon Factory Program Advisory Committee (Proposal number 2020G667). This work was financially supported by ISHIZUE 2020 of the Kyoto University Research Development Program, a Grant-in-Aid for Scientific Research (B) (21H01975), a Grant-in-Aid for Challenging Research (Exploratory, 20K21108) and a Grant-in-Aid for Young Scientists (19K15359) from the Japan Society for the Promotion of Science (JSPS), and the Program for Element Strategy Initiative for Catalysts & Batteries (ESICB, JPMXP0112101003), commissioned by the MEXT of Japan. S. P. Singh thanks the JICA for providing a scholarship under the FRIENDSHIP project to pursue his Ph.D. in Japan.

Notes and References

1 A. Hagen and F. Roessner, *Catal. Rev. - Sci. Eng.*, 2000, **42**, 403–437.
2 Y. Zhu, S. Shi, C. Wang and Y. H. Hu, *Int. J. Energy Res.*, 2020, **44**, 708–717.
3 B. G. Hashiguchi, M. M. Konnick, S. M. Bischof, S. J. Gustafson, D. Devarajan, N. Gunsalus, D. H. Ess and R. A. Periana, *Science*, 2014, **343**, 1232–1237.
4 A. E. Shilov and G. B. Shul’pin, *Chem. Rev.*, 1997, **97**, 2879–2932.
5 H. Chen, L. Li and J. Hu, *Catal. Today*, 2018, **310**, 94–97.
6 M. A. Bañares, *Catal. Today*, 1999, **51**, 319–348.
7 S. Bywater and E. W. R. Steacie, *J Chem Phys*, 1951, **19**, 326–329.
8 A. Hu, J. J. Guo, H. Pan and Z. Zuo, *Science*, 2018, **361**, 668–672.
9 K. Wada, K. Yoshida, T. Takatani and Y. Watanabe, *Appl. Catal. A, Gen.*, 1993, **99**, 21–36.
10 C. T. Brigden, S. Poulston, M. V. Twigg, A. P. Walker and A. J. J. Wilkins, *Appl. Catal. B Environ.*, 2001, **32**, 63–71.
11 R. Zhang, H. Wang, S. Tang, C. Liu, F. Dong, H. Yue and B. Liang, *ACS Catal.*, 2018, **8**, 9280–9286.
12 K. Wada, K. Yoshida, Y. Watanabe and T. Suzuki, *Appl. Catal.*, 1991, **74**, L1–L4.
13 X. T. Wang, S. H. Zhong and X. F. Xiao, *J. Mol. Catal. A Chem.*, 2005, **229**, 87–93.
14 J. Suzuki, K. Fujimoto, T. Mori, M. Watanabe and Y. Hasegawa, *J. Sol-Gel Sci. Technol.*, 2000, **19**, 775–778.
15 K. Wada, H. Yamada, Y. Watanabe and T. A. Mitsudo, *J. Chem. Soc. - Faraday Trans.*, 1998, **94**, 1771–1778.
16 T. E. Bitterwolf, D. L. Kline, J. C. Linehan, C. R. Yonker and R. S. Addleman, *Angew. Chemie - Int. Ed.*, 2001, **40**, 2692–2694.
17 L. Yuliati and H. Yoshida, *Chem. Soc. Rev.*, 2008, **37**, 1592–1602.
18 H. Yoshida, *Catal. Surv. from Asia*, 2005, **9**, 1–9.
19 Y. Kato, H. Yoshida and T. Hattori, *Chem. Commun.*, 1998,

2389–2390.
20 H. Yoshida, N. Matsushita, Y. Kato and T. Hattori, *Phys. Chem. Chem. Phys.*, 2002, **4**, 2459–2465.
21 Y. Kato, N. Matsushita, H. Yoshida and T. Hattori, *Catal. Commun.*, 2002, **3**, 99–103.
22 H. Yoshida, N. Matsushita, Y. Kato and T. Hattori, *J. Phys. Chem. B*, 2003, **107**, 8355–8362.
23 L. Yuliati, T. Hamajima, T. Hattori and H. Yoshida, *J. Phys. Chem. C*, 2008, **112**, 7223–7232.
24 L. Yuliati, T. Hattori, H. Itoh and H. Yoshida, *J. Catal.*, 2008, **257**, 396–402.
25 S. P. Singh, A. Anzai, S. Kawaharasaki, A. Yamamoto and H. Yoshida, *Catal. Today*, 2021, **375**, 264–272.
26 S. P. Singh, A. Yamamoto, E. Fudo, A. Tanaka, H. Kominami and H. Yoshida, *ACS Catal.*, 2021, **11**, 13768–13781.
27 G. Wang, X. Mu, J. Li, Q. Zhan, Y. Qian, X. Mu and L. Li, *Angew. Chemie*, 2021, **133**, 20928–20932.
28 J. Lang, Y. Ma, X. Wu, Y. Jiang and Y. H. Hu, *Green Chem.*, 2020, **22**, 4669–4675.
29 M. Ishimaru, F. Amano, C. Akamoto and S. Yamazoe, *J. Catal.*, 2021, **397**, 192–200.
30 B. Kraeutler and A. J. Bard, *J. Am. Chem. Soc.*, 1978, **100**, 5985–5992.
31 P. Michorczyk and J. Ogonowski, *Appl. Catal. A Gen.*, 2003, **251**, 425–433.
32 B. Zheng, W. Hua, Y. Yue and Z. Gao, *J. Catal.*, 2005, **232**, 143–151.
33 Y. Hou, L. Wu, X. Wang, Z. Ding, Z. Li and X. Fu, *J. Catal.*, 2007, **250**, 12–18.
34 K. Shimura and H. Yoshida, *Catal. Surv. from Asia*, 2014, **18**, 24–33.
35 F. Amano, C. Akamoto, M. Ishimaru, S. Inagaki and H. Yoshida, *Chem. Commun.*, 2020, **56**, 6348–6351.
36 K. Shimura, T. Yoshida and H. Yoshida, *J. Phys. Chem. C*, 2010, **114**, 11466–11474.
37 L. Yuliati, H. Itoh and H. Yoshida, *Chem. Phys. Lett.*, 2008, **452**, 178–182.
38 L. Meng, Z. Chen, Z. Ma, S. He, Y. Hou, H. H. Li, R. Yuan, X. H. Huang, X. Wang, X. Wang and J. Long, *Energy Environ. Sci.*, 2018, **11**, 294–298.
39 X. Y. Wu, Z. Tang, X. Zhao, X. Luo, S. J. Pennycook and S. L. Wang, *J. Energy Chem.*, 2021, **61**, 195–202.
40 Z. Yi, Z. Tang, X. Wu, A. Huang, X. Luo, G. Q. Xu, Y. Zhu and S. L. Wang, *Appl. Catal. B Environ.*, 2021, 120919.
41 S. Park, J. Jeong, K. I. Fujita, A. Yamamoto and H. Yoshida, *J. Am. Chem. Soc.*, 2020, **142**, 12708–12714.
42 S. Y. Lee and S. J. Park, *J. Ind. Eng. Chem.*, 2013, **19**, 1761–1769.
43 K. Nakagawa, C. Kajita, Y. Ide, M. Okamura, S. Kato, H. Kasuya, N. Ikenaga, T. Kobayashi and T. Suzuki, *Catal. Letters*, 2000, **64**, 215–221.
44 P. Berteau, C. Ceckiewicz and B. Delmon, *Appl. Catal.*, 1987, **31**, 361–383.
45 Y. P. Pérez, F. T. Morales, R. P. Hernández, R. A. Murillo, P. A. Peña and R. G. Romero, *Fuel*, 2017, **198**, 11–21.
46 F. Tzompantzi, Y. Piña, A. Mantilla, O. A. Martínez, F. G. Hernández, X. Bokhimi and A. Barrera, *Catal. Today*, 2014, **220–222**, 49–55.
47 H. Li, Z. Bian, J. Zhu, Y. Huo, H. Li and Y. Lu, *J. Am. Chem. Soc.*, 2007, **129**, 4538–4539.
48 S. Wang, Y. Gao, S. Miao, T. Liu, L. Mu, R. Li, F. Fan and C. Li, *J. Am. Chem. Soc.*, 2017, **139**, 11771–11778.
49 M. A. Saqlain, A. Hussain, M. Siddiq, A. R. Ferreira and A. A. Leitão, *Phys. Chem. Chem. Phys.*, 2015, **17**, 25403–25410.
50 M. Horn, C. F. Schwerdtfeger and E. P. Meagher, *Zeitschrift für Krist.*, 1972, **136**, 273–281.
51 W. H. Baur and A. A. Khan, *Acta Cryst.*, 1971, **27**, 2133–2139.
52 E. A. Owen and E. L. Yates, *London, Edinburgh, Dublin Philos. Mag. J. Sci.*, 1933, **15**, 472–488.
53 K. Kimura, S. I. Naya, Y. J. Nouchi and H. Tada, *J. Phys. Chem. C*, 2012, **116**, 7111–7117.
54 V. Schwartz, D. R. Mullins, W. Yan, H. Zhu, S. Dai and S. H. Overbury, *J. Phys. Chem. C*, 2007, **111**, 17322–17332.
55 S. Jo, P. Verma, Y. Kuwahara, K. Mori, W. Choi, and H. Yamashita, *J. Mater. Chem. A*, 2017, **5**, 21883–21892.
56 A. Tanaka, S. Sakaguchi, K. Hashimoto and H. Kominami, *ACS Catal.*, 2013, **3**, 79–85.
57 A. Tanaka, K. Hashimoto and H. Kominami, *J. Am. Chem. Soc.*, 2012, **134**, 14526–14533.
58 D. Mateo, N. Morlanes, P. Maity, G. Shterk, O. F. Mohammed and J. Gascon, *Adv. Funct. Mater.*, 2021, **31**, 2008244.
59 D. Takami, A. Yamamoto and H. Yoshida, *Catal. Sci. Technol.*, 2020, **10**, 5811–5814.
60 K. Takeda, A. Yamaguchi, Y. Cho, O. Anjaneyulu, T. Fujita, H. Abe and M. Miyauchi, *Glob. Chall.*, 2020, **4**, 1900067.
61 Q. Xie, T. Lei, C. Miao, W. Hua, Y. Yue and Z. Gao, *Catal. Letters*, 2020, **150**, 2013–2020.
62 G. A. Skorobogatov, B. P. Dymov, Y. I. Pogosyan, V. K. Khripun and E. P. T. Roux, *Russ. J. Gen. Chem.*, 2003, **73**, 75–84.